Journal of Disability Research

2022 | Volume 1 | Issue 1 | Pages: 2–11
DOI: 10.57197/JDR-2022-0003

The Structure and Mechanical Properties of Type IV Collagen in Lens Basement Membrane: Deterioration with Age and Glycation Reviewed

D. A. Bradley

Center for Applied Physics and Radiation Technologies, School of Engineering and Technology, Sunway University, 47500 Bandar Sunway, Selangor, Malaysia

Correspondence to: D. A. Bradley
E-mail: dbradley@sunway.edu.my

Published Online: November 29 2022

ABSTRACT

Biomedical physics seeks to confront the amazingly intricate sets of interlinked processes that when in synchrony sustain life. In so doing, questions arise regarding the functionality of cells, organised tissues and organs and the myriad interactional processes required, and also as to how the onset of disease limits viability and what possible repair processes can be caused to happen, including in biosynthetic routes. It is clearly a multidisciplinary field providing a multi-pronged array of endeavours, bringing into play concepts and tools within the armoury of physics, chemistry, engineering, mathematics, and all of the applied areas that arise from these. As expected, the pursuit is beset by ignorance and in the absence of a polymath, the ability to progress is clearly a team effort. Not least among the challenges are that oftentimes the medium under investigation no longer enjoys the vitality of life, including when using *in vitro* techniques acknowledging that in excised tissues repair processes are clearly inoperative. As such, questions inevitably arise as to whether the results of an investigation bear resemblance to that of the living entity. Here, we will focus on just one example of such a pursuit, namely investigations of degraded vision arising from alterations in the basement membrane (BM). We address alterations that may arise from diabetes and ageing, which are changes that bring about life-altering disability. In examining this one area of biophysical investigation, we hope that the reader will gain a degree of appreciation of the need for such studies even if, as here, we simply represent just one particular aspect of what are clearly complex areas. At the outset, we simply mention that the BM forming the eye lens capsule is a highly specialised form of extracellular matrix in which the major structural element is a network of type IV collagen. Changes in the structure and mechanical properties of the BM are believed to be associated with the pathophysiology of ageing and diseases, including diabetes and cancer.

KEYWORDS

Basement Membrane, Lens, collagen-4

INTRODUCTION

One area of biophysical investigation concerns organised tissues. Here we present the example of the basement membrane (BM), a ubiquitous and highly specialised form of extracellular matrix. The work presented herein arises from the study of Layla Ali, carried out at Exeter University, supervised by the present author (Ali et al., 2004).

BM is a key element in the processes of differentiation and growth and in the mature animal acts as a filter and a mechanical support. Most notably, it underlies the endothelial cells throughout the vasculature providing mechanical support and acting as a filter to the movement of water and solutes. This is particularly evident in the kidney, albeit essential to homeostasis throughout the body.

Here, the area to be illustrated concerns an examination of lens tissue beset by various degrading processes. For the BM forming the capsule of the lens, this can arise both during diabetes and ageing, leading to a manifest reduction in the clarity of vision. In our endeavours, we investigated the structure and mechanical properties of the BM of the equine lens capsule and the changes associated with age and *in vitro* glycation; here we detail some of the findings from such studies, including those obtained through structural analysis using synchrotron-based small- and wide-angle X-ray scattering (the so-called WAXS and SAXS diffractional techniques). We also show the results of Raman microspectrometry, the latter looking at biochemical-level alterations. Finally, we show results from static, dynamic and thermo-mechanical testing. All of these are used to look at intact tissues and tissues after selective extraction of various proteins that may mask findings.

As we will see, the findings include those from X-ray scattering patterns in hydrated tissue, features being observed

that are associated with the helical, NC1 and 7S domains and a four-point pattern associated with cybotactic nematic organisation—matters that were only previously observed in mature, dehydrated tissue subjected to prolonged strain. The structures observed here are anisotropic in young, unstrained tissue and also show a number of changes induced by strain. In older tissue, a similar pattern is evident in strained tissue, but relaxed tissue is symmetric, with its structure being difficult to resolve.

In vitro glycation of young tissue has reproduced many features characteristic of more aged tissue. The use of Raman microspectrometry has revealed the secondary structure of type IV collagen to be different from that of the fibrous collagens. Spectra from glycated tissue show specific interactions with sugar residues and structural changes. Mechanical strain has not been found to affect Raman peak positions or secondary structure but has altered the polarisation of the spectrum. Finally, mechanical testing has confirmed the non-linear viscoelastic properties of BM. Glycoproteins and proteoglycans contribute to the initial modulus and viscous properties but the ultimate modulus is determined by the collagen network. Both initial and final moduli decrease with age but, because of an increase in thickness, whole-tissue properties remain relatively constant. *In vitro* glycation has been found to increase the elastic modulus but to reduce the viscous fraction and is also associated with an increase in thickness.

BACKGROUND OF THE BASEMENT MEMBRANE

The major constituents of BM are type IV collagen, constituting up to 40% of the dry weight of the tissue, laminin, heparan sulphate proteoglycans and entactin/nidogen (Kefalides, 1971; Timpl, 1989). Electron microscopy reveals a three-dimensional network of fibres, formed by anastomosing of irregular strands averaging 4 nm in thickness (Inoue et al., 1983). The fibres consist of a core filament of type IV collagen surrounded by a sheath containing the other BM components to form a ribbon-like structure (Yurchenko and O'Rear, 1993; Inoue, 1994). Collagen IV, therefore, forms the skeleton of the BM structure and different models of its supramolecular organisation have been proposed (Yurchenco and Furthmayr, 1984; Barnard et al., 1987), although unequivocal evidence in favour of a particular model is still lacking.

Changes in the structure and function of the BM occur in ageing and are implicated in diseases ranging from cancer to diabetes. In the latter context, it is hypothesised that non-enzymatic glycation of the BM is responsible for some of the vascular dysfunctions that are major complications of diabetes (e.g. Banga and Sixma, 1986; Basta et al., 2004). There have been a number of studies showing that non-enzymatic glycation modifies the functional properties of extracellular matrix components. Because the reaction rate is relatively low, the most stable components of the matrix, such as collagen and elastin, are most susceptible to its effects. A number of studies have reported that glycation alters the structure and mechanical properties of type I collagen (e.g. Menzel and Reihsner, 1991) and elastin (Winlove et al., 1996), but to our knowledge there has been very little work on type IV collagen.

In light of information, the initial intention was to investigate the effects of glycation on the structure and mechanical properties of BM, using the equine lens capsule as a source of BM in a form suitable for mechanical testing and structural analysis. The lens offers a relatively thick BM, much easier to handle than, for instance, the less thick BM of the nephrons of the kidney (another of the tissues that functionally degrade in the presence of diabetes). Figure 1 shows a schematic cross-section of the lens of the human eye, with a measure of the BM thickness also being provided.

In order to relate mechanical measurements to matrix and molecular structures in the present study, we have used a combination of WAXS and SAXS and Raman microspectrometry. We suggest that the latter technique has not been previously applied to BM, while X-ray scattering certainly has (Gathercole et al., 1989); Figure 2 relates the X-ray

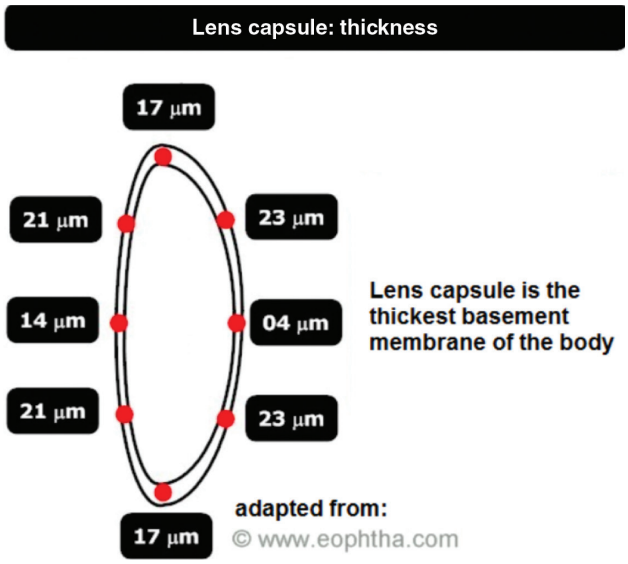

Figure 1: Cross-section of the lens of the mature human eye, with an indication of the typical thickness of the lens capsule formed in the basement membrane. Adapted from eophtha.com.

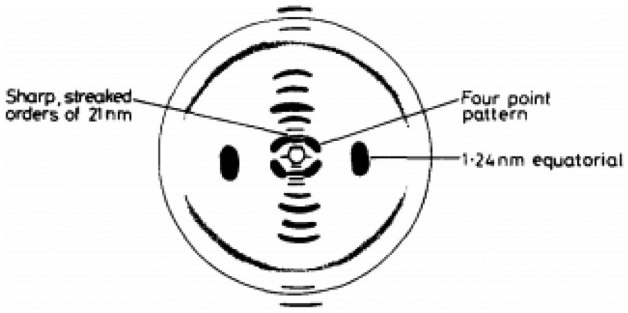

Figure 2: Schematic of the results of Gathercole et al. (1989) obtained for an extracted bovine lens capsule; the authors indicate the major meridional reflections, also drawing attention to the overall similarity with the organisation of a cybotactic nematic liquid crystal.

diffraction results of the study by Gathercole et al. (1989). It is noted that at the time of their investigations, far greater use was being made of film in order to capture images, two-dimensional (2D) digital cameras having yet to make a strong appearance; hence the authors made use of a schematic in order to depict the features observed in the actual film images that they obtained (film results typically being reproduced rather poorly in print).

Following the protocol, as guided by the study by Gathercole and others at the University of Bristol, in preliminary experiments we found inconsistent diffractional behaviour which we were finally able to attribute to an effect of age on the tissue structure. It therefore became necessary to include age as an additional factor in the design of our experiments, and it also proved to influence mechanical properties.

METHODS

Tissue samples

Fresh horse eyes covering the age ranges 0-5 (young), 10-15 (mature), and 20-25 years (old) were obtained from an abattoir. The cornea and iris were removed and the lens was released by carefully lifting and cutting through the zonular fibres. An incision was then made around the lens to isolate the capsule from the lens fibres. The capsule was dissected as a disc and washed extensively in phosphate buffered saline (PBS) to remove any adherent material. The disc was subsequently cut into vertical strips, each 2 mm wide. Only the central part of the lens capsule was used to avoid contamination with zonular fibres.

For some experiments, matrix components were selectively extracted from the tissue using a number of protocols. Proteoglycans and other glycoproteins were removed either by digestion for 20 h with heparinase (5 units/ml, Sigma, UK) and hyaluronidase (1 mg/ml, Type 1S, Sigma, UK) (Heinegard and Sommarin, 1987), or with 4 M guanidinium chloride (GuHCl) (Fisher Biotech, at 20C for 10-20 h) (Paulsson et al., 1987). The effects of disulphide bond cleavage were investigated after incubation in 20 mM dithiothreitol (DTT, Fisher Biotech) for 20 h (Barnard and Gathercole, 1991). After extraction, the samples were washed for 1-3 h with PBS containing a cocktail of protease inhibitors: 2 mM N-ethylmaleimide, 0.5 mM phenylmethylsulfonyl fluoride and 4 mM ethylenediamine tetraacetic acid (Yurchenco and Ruben, 1987).

Ribose was used for *in vitro* glycation to increase the reaction rates. In order that the effects of glycation could be compared with control tissue from the same capsule, proteoglycan-depleted anterior capsules were divided into four strips. One section was placed in PBS containing sodium azide as a preservative at 37°C and used as a control. The three remaining sections were placed in the same buffer containing 200 mM ribose and incubated for 2, 6, and 12 weeks. After the required incubation time, the lens capsules were removed from the incubation medium and extensively washed in PBS before use.

X-ray diffraction and scattering

In an initial series of experiments, the protocol of Barnard et al. (1987) was followed in which strips of BM were subjected to a constant load of 0.15 N for 48 h, generating a strain of about 50-55% under high relative humidity and then air dried before the X-ray diffraction measurement. In some experiments, tissues were rehydrated before measurement by sealing in a 2-mm glass capillary at 100% humidity. For later experiments, a micro-manipulator-controlled loading rig was constructed which could be mounted on the synchrotron beamline and allowed samples to be strained by 20-60% of their initial length at the time of testing, with the sample hydration being maintained by a wick coupling the lower end of the sample to a water reservoir. This approach was necessary because humidity chambers constructed even of the thinnest available mylar produced scattering comparable to that from the samples themselves. For small-angle scattering, where scattering intensity was low, either a bundle of strips or a whole disc, rolled up before uniaxial loading, was used.

Measurements were made at the Synchrotron Radiation Source at Daresbury in the UK (this Warrington-based facility has now been superseded in the UK by the DIAMOND Synchtotron, a facility based in Oxfordshire). For wide-angle measurements (WAXS), Station 14.1 at the Daresbury synchrotron was used, providing a beam of wavelength 0.149 nm and 100 × 100 μm in area. The sample was positioned to ensure that the beam passed through the centre of the strip. The sample-to-detector distance ranged from 15 to 20 cm, allowing *d*-spacings up to 7.0 nm to be resolved. The exposure time was typically 5 min. The system was calibrated using the 0.372 nm and 0.414 nm X-ray reflections from paraffin wax. SAXS measurements were performed on Station 2.1. The X-ray beam, of wavelength 0.154 nm, had a vertical height of 0.5 mm and a width of 1.5 mm at the sample, which was placed normal to the beam. The detector tube length was 1.25 m and a multi-wire gas proportional area detector was used to obtain the 2D patterns, as desired. The system was calibrated using silver behenate (*d*-spacing of 5.838 nm). 2D SAXS patterns were reduced to one-dimensional (1D) profiles by sector integration with respect to the meridional/equatorial axes and displayed as a function of the modulus of the momentum transfer (depending on the scattering angle and X-ray wavelength). A 1.25-m camera set-up allowed for a momentum transfer interval of $0.0063\ Å^{-1} < s < 0.10000\ Å^{-1}$ to be covered. An exposure time of 30 min was generally sufficient. Images were acquired in a frame-refresh mode (typically 5 min per frame for six frames). In this mode, it was possible to monitor for changes in structure due to radiation damage. This was observed in several hydrated samples following protracted exposure. Only frames showing no such changes were averaged and used in the subsequent data analysis. Data from both the WAXS and SAXS experiments were analysed using the software packages, FIT2D (Hammersley, 1998) and OTOKO (Bendall et al., 1985), respectively.

Raman microspectroscopy

Spectra were acquired using a Renishaw (UK) 1000 Raman Microscope system equipped with a 100-mW helium-neon

(HeNe) near-infrared laser (785 nm excitation). Calibration was carried out using the 520.4 cm^{-1} line of a silicon wafer. The strip of lens capsule was mounted in a purpose-made rig, similar to that used in the diffraction measurements, in which one arm was attached to a micrometre screw and the other was fixed allowing the application of uniaxial strain. In the majority of measurements, the specimen lay in a thin film of PBS between an aluminised microscope slide on the lower surface and a quartz cover slip, although some measurements were also made on dry tissue. Raman spectra were obtained using a 40 or 50 objective focused on the sample to give an analysis area of approximately 20 μm^2. Data were collected over 30 s at a laser power of 10 mW and seven acquisitions were accumulated to improve the signal-to-noise ratio. No effects of radiation damage were observed under these conditions. All reported spectra are the means of measurements on six tissue samples. In experiments where the effects of strain were examined, the specimen was realigned visually after each application of strain to ensure that the measurements were made at the same point in the specimen at all strains.

For polarisation measurements, a half-wave plate could be introduced into the incident beam and rotated to produce a beam that was polarised parallel or perpendicular to the long-axis of the sample. A half-wave plate and polariser in the scattered beam allowed the acquisition of scattered light of either polarisation.

Data analysis, including background subtraction using a cubic spline fit and amide band analysis, were performed using the Wire/LABSPEC (Renishaw) software. Determination of a secondary structure from the amide I band essentially followed the procedures of Sane et al. (1999). Polarised spectra were acquired for all combinations of polarisation of the incident and scattered radiation. Two intensity ratios $\rho_{\parallel} = I_{zx}/I_{zz}$ and $\rho_{\perp} = I_{xz}/I_{xx}$ were calculated where, in a coordinate system in which the specimen lay in the x–z plane oriented along the z-axis, I_{ij} refers to the peak intensity when the exciting beam is polarised in the i-direction and the scattered beam is measured with the filter transmitting in the j-direction.

Mechanical testing

A custom-made uniaxial tensile testing apparatus was employed in which the ends of the lens capsule strip were sandwiched between small pieces of finely graded sand paper and clamped in two sets of jaws. The upper jaws were attached to a force transducer (TRN 001, range 0.05-0.2 N, Kent Scientific Corp.) and the lower jaws were mounted on a movable lower arm connected to a micrometre screw driven by a stepper motor (Radiospares, UK), with the displacement being measured by a displacement transducer (Research Instruments Ltd., UK). Force and displacement were logged using Picolog software (Picolog, UK). The specimen was immersed in a bath of PBS, pH 7.4, thermostatically controlled to a temperature of 25°C throughout testing.

Each lens capsule provided four 2-mm-wide strips for testing. In preliminary experiments to investigate the homogeneity of the tissue, strips cut from different locations in the lens capsule were compared. To investigate isotropy, measurements were made on paired samples cut in orthogonal directions. Specimen thickness was measured microscopically by focusing on glass microspheres adhering to the upper and lower surfaces of the lens capsule. The thickness and the width were measured using the travelling microscope at different locations and the mean of these was used to determine the cross-sectional area of the specimen. Stress was calculated as load per unit macroscopic cross-sectional area. Strain was determined relative to the relaxed length of the specimen.

Quasi-equilibrium stress–strain curves were determined at a strain rate of 0.04 mm/s. Five to seven cycles up to a maximum strain of 20% were performed to allow for preconditioning, with the data being used only from the last cycle. Viscoelastic properties were investigated both by exploring the effects of strain rate in the range of 0.007-0.7 mm/s and by measuring the time course of relaxation following instantaneous application of a 10% strain. The latter data were fitted to the Maxwell model, implemented in Kaleidagraph (Synergy Software).

Thermomechanical testing employed an apparatus and protocols developed at the University of Exeter. The specimen was loaded quasi-statically to a strain of 0.5% at a starting temperature of 22.5°C. The change in length at constant force was then monitored as a temperature ramp of 1°C/min was applied, up to a temperature of 80°C.

RESULTS

X-ray scattering

Early results from this study were reported by Ali et al. (2004). Here the X-ray experiments have been extended and complemented with additional biophysical studies. In addition to the dried, pre-strained, young tissues previously studied by Barnard and Gathercole (1991), we obtained scattering patterns from hydrated tissues of a range of ages under differing strains.

Dehydrated, strained tissue

The WAXS pattern in Figure 3 was obtained from a mature specimen, following the protocol of Barnard and Gathercole, showing the features that had previously been reported by the Bristol group.

The strong meridional arc at a spacing of 0.285 nm shown for young tissue (Fig. 4a) corresponds to the amino acid spacing along the collagen triple helices and a weaker reflection at 0.900 nm reflecting the pitch of the triple helix, as well as features arising from supramolecular structures. Meridional reflections, which Barnard and Gathercole attributed to 8 nm bundles formed from overlapping domains, were indexed to 27 nm rather than the 21 nm they reported. The four-point pattern that Barnard and Gathercole interpreted as a cybotactic, nematic arrangement with a *d*-spacing of 3.9 nm is clearly evident (Fig. 4b).

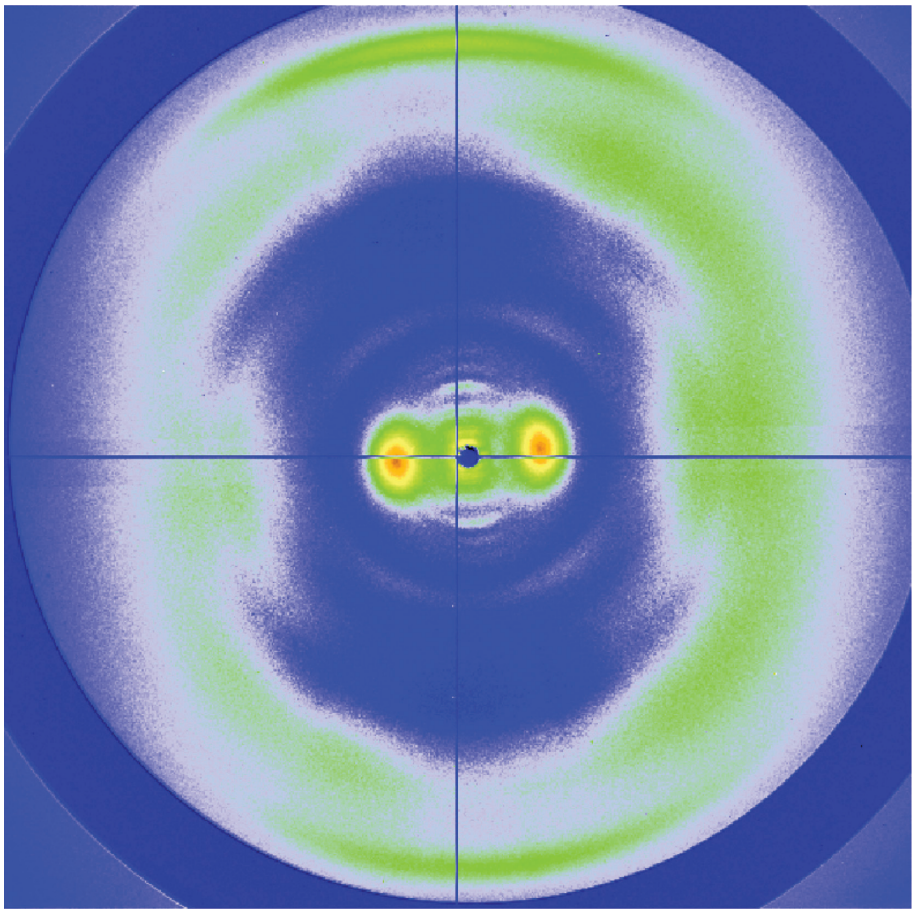

Figure 3: Typical WAXS pattern of a stretched, dried equine lens capsule of a mature animal, showing meridional and equatorial arcs. The dark spot at the centre of the pattern is a result of the use of a beam stopper, the purpose of which is to radically attenuate the direct (unscattered) beam. Abbreviation: WAXS, wide-angle X-ray scattering.

The SAXS imaging of Figure 4 reveals higher orders of these structures and adds a meridional reflection at approximately 95 nm, also noted by Gathercole and Barnard.

When the tissue was depleted of proteoglycans and glycoproteins, the background scattering was reduced, but there was no significant change in *d*-spacing. Following disulphide bond cleavage with DTT, the meridional reflections ascribed to the 7S domain became more diffuse. This lent confidence to the attribution but no quantification of the changes was attempted because of the poor resolution of the peaks against the high background.

Effects of age in hydrated, pre-strained tissue

Hydrated tissue gave a much higher background and consequently poorer peak resolution than dehydrated samples, but no significant differences in structural parameters could be discerned. In young (0-5 years) and mature (10-15 years) animals, scattering patterns could be resolved in unstrained tissue. As shown in Figure 4a, the patterns from the young tissue showed the asymmetries we have described above for mature, strained tissue. However, with increasing age, the patterns became increasingly symmetric and diffuse (Fig. 5).

In the oldest animals, we were generally unable to resolve any structure. In addition, there were changes in *d*-spacings with age. The most significant effect was on the lateral spacing of the collagen and the half-width of its peak. While there were significant differences between the age groups, no trend with age was discernible.

Effects of strain

These effects were investigated in young (0-5 years) tissue, where better peak resolution could be achieved. As strain increased up to 50%, the meridional reflections became sharper and additional broad peaks became apparent at larger scattering angles (Fig. 6). This shows the results in tissue from a 2-year-old animal.

Effects of glycation

The effects of glycation were investigated in strained, mature proteoglycan-depleted tissue. Changes were evident in both the WAXS and SAXS patterns, to an extent that increased with the period of glycation. In some specimens, the four-point pattern was lost or overlaid by a diffuse ring that obscured many sharp reflections. The most consistent observation was an increase in the equatorial *d*-spacing with

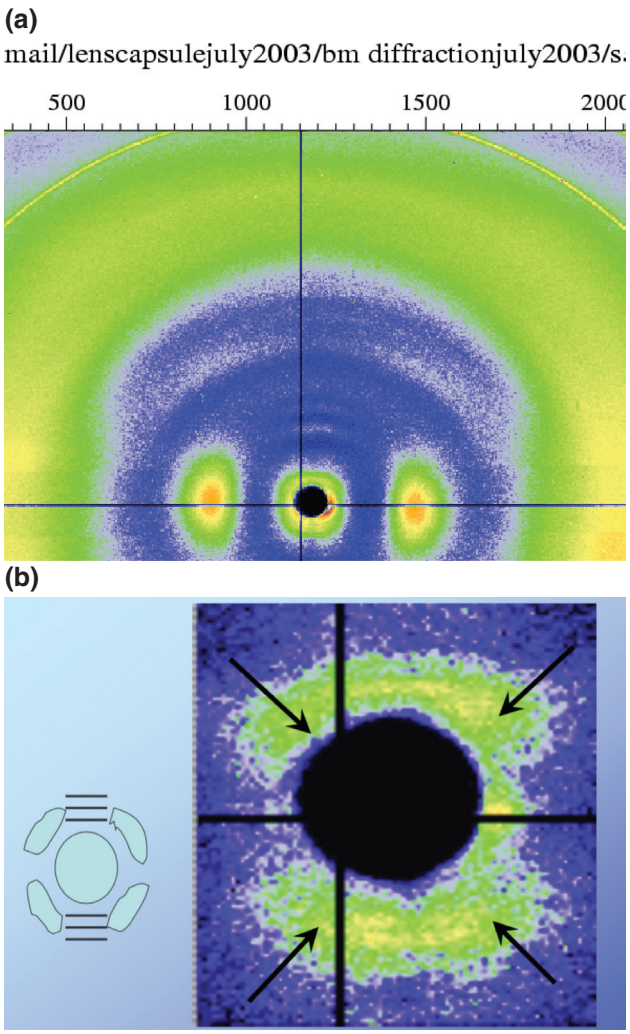

Figure 4: (a) SAXS 2D pattern of dry, stretched lens capsule from young tissue taken at a particular sample-to-detector distance. (b) Off-meridional "four-point" patterns at 43 degrees with *d*-spacing of 3.82 nm (the schematic to the left hand side indicates the arrangement in a less photon-starved situation). Refer to Figure 2 to see a comparison with the results of the group of Gathercole. Abbreviation: 2D, two-dimensional; SAXS, small-angle X-ray scattering.

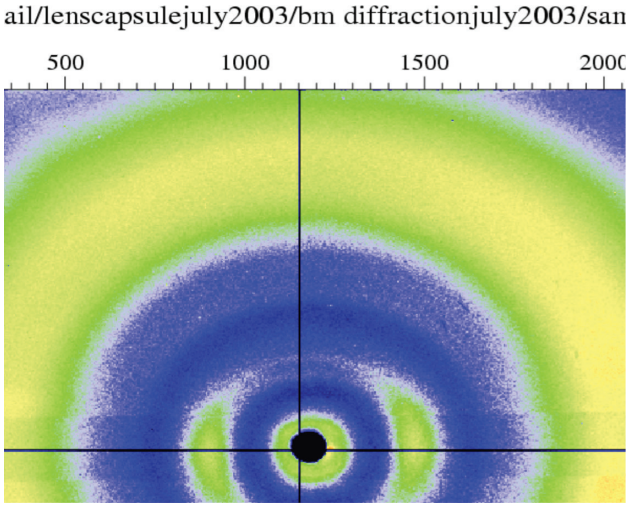

Figure 5: SAXS 2D pattern of dry, stretched lens capsule from tissue of an older equine sample, the pattern being obtained at the sample-to-detector distance as that for Figure 4a. Abbreviation: 2D, two-dimensional; SAXS, small-angle X-ray scattering.

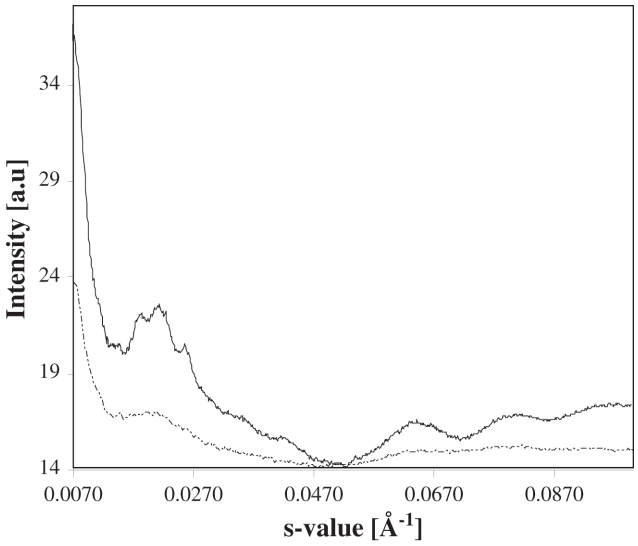

Figure 6: Comparison of meridional scattering patterns in relaxed tissues (the dashed curve) and following imposition of 50% strain (revealing an emergence of structural detail with strain). The s-value represents the momentum transfer.

incubation time (Fig. 7). The peaks in the SAXS pattern associated with the NC1 domain also became progressively broader and less well resolved with increasing incubation time (not shown). The overall effect of these changes was that at long incubation times the patterns came closely to resemble those of old tissue.

Raman microspectrometry

Figure 8 shows the averaged Raman spectra obtained from seven samples of young equine lens capsules at relaxed length and fully hydrated.

Extraction of proteoglycans and glycoproteins did not significantly change the spectrum, demonstrating that it is dominated by the contribution from the collagen. The type IV collagen spectrum is similar to that reported for gelatine and type I collagen (e.g. Frushour and Koenig, 1975, where peak attributions may be found), reflecting the broad similarities in amino acid composition. Evidence of extensive disulphide bonding is seen in the peaks at 540 and 512 cm^{-1}. Raman spectroscopy can be used to measure changes in the overall folding of a protein resulting from treatment. The amide I region of Raman spectra (1600-1700 cm^{-1}) is used extensively to characterise the secondary structure of proteins and polypeptides. The figure displays a primary band at 1650 cm^{-1} assigned to an α-helical structure (67.8% of peak area in amide I region). There is also a smaller band at 1617 cm^{-1} assignable to the β-structure (22% of peak area)

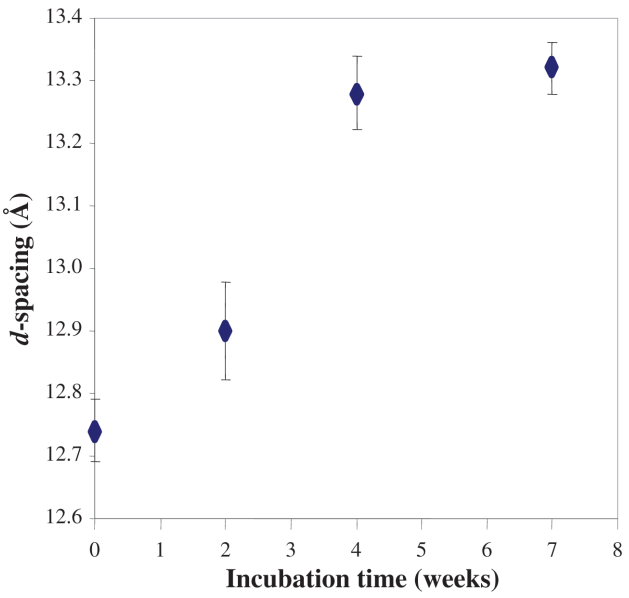

Figure 7: The effect of prolonged incubation time on *d*-spacing.

and a small contribution for β-structure or unordered regions at 1671 cm^{-1} (4.6% of peak area).

Treatment leads to significant changes in the amide I region. The largest peak is still the 1650 cm^{-1} α-helical band, but it shows a decreased relative intensity (49.8% of the peak area). A small decrease is also observed in the β-structure band at 1616 cm^{-1} (14.6% of peak area); however, the unordered band at 1666 cm^{-1} (28.8% of peak area) increases in intensity compared to the Raman spectrum of the untreated sample. A new prominent band at 1640 cm^{-1} appears in the treated sample, which we assign to the CO stretch for new amide bonds formed between Glu and Lys side chains from the cross-linking reaction; the appearance of a 1640 cm^{-1} band is also observed in other treated proteins. The amide I band shows differences in the secondary structure to the fibrous collagens and decomposition suggests that 48% of the structure is unordered helices and sheets, 39% β-turns and only 7% α-helix. The secondary structure was unaffected by glycoprotein and proteoglycan removal and the spectrum did not change with the age of the tissue.

Spectra in young tissue in a relaxed state and at strains up to 50% showed no significant changes in peak positions (± 2 cm^{-1}) or amide band structure. The spectrum was polarisation-sensitive, even in relaxed tissue, particularly with respect to the tyrosine and phenylalanine peaks (ratio of $\rho_{\parallel}/\rho_{\perp} = 7.14$ for tyrosine and 6.25 for phenylalanine). The ratio changed with the strain, in a manner qualitatively consistent with the vibrations aligning themselves with the direction of stretch. No quantification was attempted, with the movement of the sampling point under strain introducing unacceptable errors.

In Figure 8, data are shown from young, proteoglycan-depleted tissue, subsequently glycated *in vitro* before examination and washed extensively. The spectrum of ribose in solution are also shown. A number of changes in the spectrum of the glycated collagen are seen. Some peaks, such as that at 510 cm^{-1}, have clear counterparts in the ribose spectrum and may arise from unreacted ribose remaining bound to the fibres even after washing, whilst others (e.g. 605 and 810 cm^{-1}) are new and probably represent reaction products or changes in the collagen structure. The latter are evidenced by a change in shape of the amide I band. Decomposition suggests that this change represents an increase in the proportion of unordered structures.

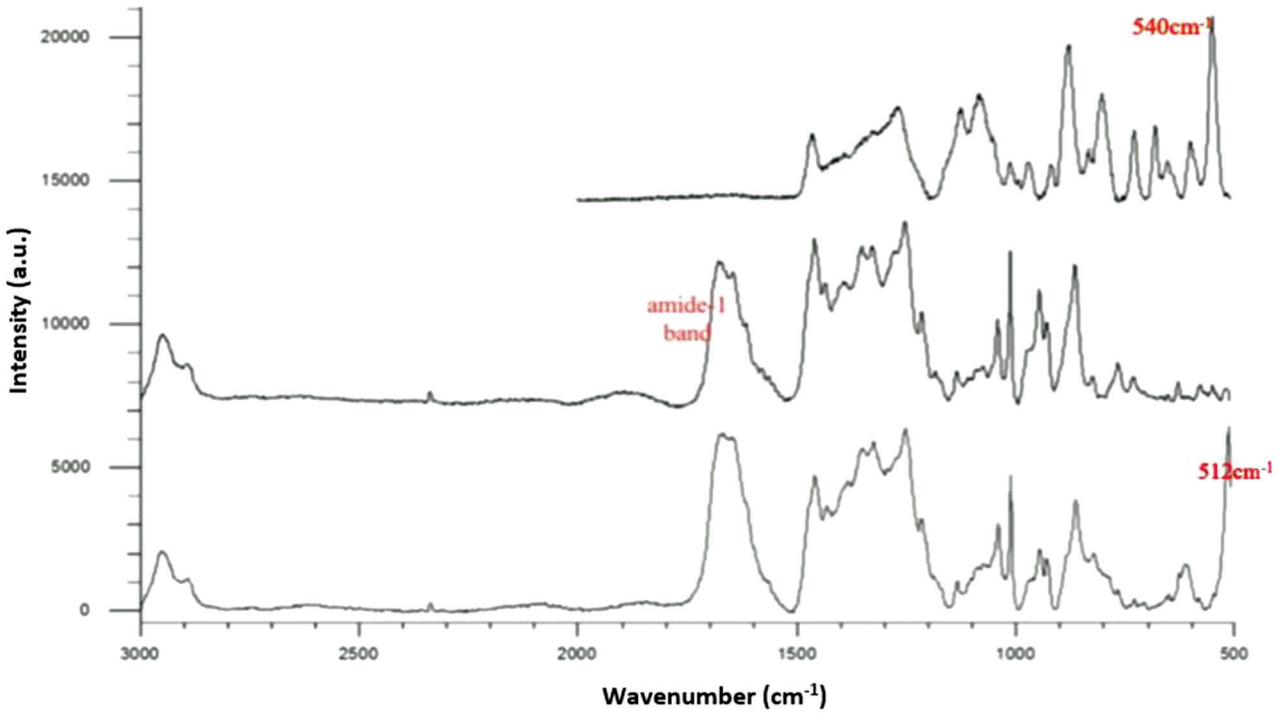

Figure 8: Raman spectrum of GuHCl-extracted basement membrane (centre spectrum) and after glycation (4 weeks, 200 mM ribose) (lower spectrum). The upper spectrum is that for the ribose alone. Abbreviation: GuHCl, guanidinium chloride.

Mechanical testing

The mechanical behaviour of the lens tissue was found to be qualitatively similar at all ages. The stress–strain curves exhibited markedly non-linear behaviour, and no anisotropic behaviour could be resolved. As illustrated in Figure 9, there was a toe-region extending in young tissue to approximately 20% strain, after which the tissue stiffened markedly.

The strain at failure was in excess of 60%, but failure generally occurred at the clamps and therefore probably reflected the method of attachment rather than intrinsic mechanical properties. Viscoelasticity was evident in steepening of the stress–strain curve with the strain rate. *In vitro* glycation modified the mechanical properties of young tissue. The magnitude of the effect depended both on the concentration of ribose in the incubation medium and the time of incubation.

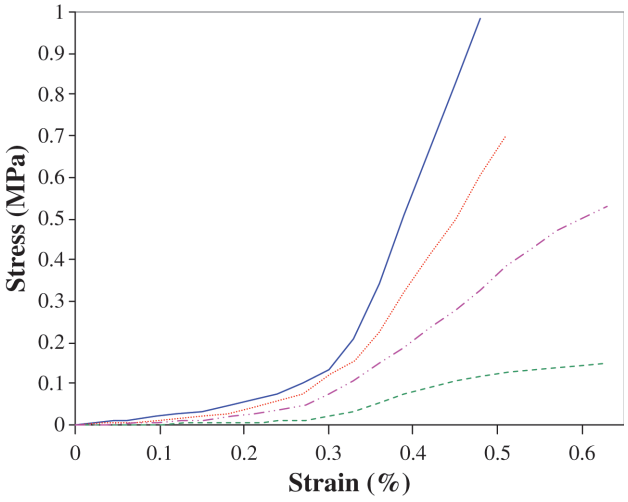

Figure 9: Progressive effect of age (starting from the lower curve for a 2-year-old animal, through 12, 17 and 24 years of age) demonstrated in reduction in the rate at which stress relaxation takes place.

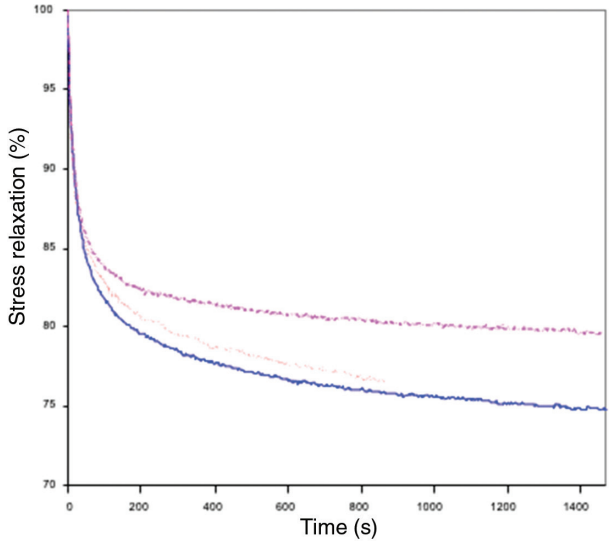

Figure 10: An equivalent relaxation curve to that of Figure 9.

DISCUSSION

The initial motivation for the present work was to investigate relationships between mechanical properties and structure in the BM of lenses. However, in preliminary experiments it was found that both structure and mechanical properties changed with age and this somewhat complicated the study. The former realisation came about largely because improvements in detector sensitivity allowed us to extend the X-ray scattering investigation beyond the dried, stretched tissue that had been investigated previously (Gathercole et al., 1989; Barnard et al., 1991). This limitation had led to questions concerning the biological relevance of the previous observations. However, we were largely able to confirm them in hydrated tissue and demonstrate consistent changes with age and mechanical strain.

In the pre-stretched, dried tissue, the meridional pattern is composed of three sets of peaks along the direction of stretch. The first are broad but can be assigned to a *d*-spacing of 6.3 nm. This corresponds to the layer spacing in collagen IV networks (Fisher, 1969) but could alternatively arise from globular structures such as the NC1 domains. These domains are in the form of an ellipsoid 6.5 7.0 10.0 nm. The second set of meridional reflections are sharp and index to a *d*-spacing of 27 nm, rather than the 21 nm reported by Barnard et al. (1987). These are thought to relate to the length of the 7S domain and our value is closer to the results from molecular modelling (30 nm Timpl et al., 1989; 26 nm Siebold et al., 1987; Timpl and Dziadek, 1986). However, the 27-nm reflection might also relate to a supercoiled super-helix with this pitch (Rippe et al., 1997). The third pattern indexed to an axial repeat of approximately 95 nm, as noted by Barnard and Gathercole (1991), and may relate to the lateral association of the NC1 domain and its binding to the long helical region of type IV collagen at intervals of approximately 100 nm (Tsilibary and Charonis, 1986) or be a repeat of a much greater range order resulting from supercoiling and interwinding of collagen strands. The only resolvable feature in the equatorial pattern corresponded to an average spacing of 1.29 nm, which corresponds to the distance of the closest approach of collagen molecules in the dry state (Brodsky and Eikenberry, 1985). The four-point pattern together with a diffuse equatorial spot is characteristic of a cybotactic nematic group (Vries, 1970). Applying this model to our data, we find a *d*-spacing of 3.94 nm and a unit length of 5.23 nm with an angle of orientation of 41 degrees. The diffuse nature of the pattern indicates that the groups cluster only in small units or otherwise reduce the order. When the sample is rotated, the change in effective *d*-spacing causes the pattern to overlap the sharp meridional reflection from layer lines of 4.49 and 5.23 nm, and this was noted in some of our preparations.

The aforementioned attributions were supported by the measurements on digested tissues. Extraction of proteoglycans and glycoproteins caused an increase in packing density and a decrease in intermolecular separation, consistent with their perceived functions in determining the organisation of the extracellular matrix. GuHCl treatment also altered scattering assigned to the NC1 domain and could reflect the strong association of proteoglycans with this region.

Cleavage of disulphide bonds with DTT was expected to loosen intermolecular associations and this effect was most evident in the 7S domain.

Hydration of the tissue greatly increased background scatter but produced no significant changes in the principal *d*-spacings.

Raman spectroscopy showed that other aspects of molecular geometry were preserved in the dehydrated tissue and also showed that in fact a considerable quantity of structural water was still present in the dried tissue (data not shown). The spectroscopy further underpinned the X-ray analysis by showing that the secondary structure of the collagen IV was unaffected by any of the extraction procedures.

One of the most striking observations was that young tissue displays very similar structural anisotropy to older tissue under strain, but this natural anisotropy is lost with age. The anisotropy, which is not allowed for in current models of BM structure, is presumably an adaptation to the stresses exerted on the tissue *in vivo*. The loss of anisotropy with age is accompanied by broadening of the scattering peaks to the extent that in old animals no pattern could generally be resolved. Ageing was also associated with changes in equatorial *d*-spacings. No simple dependency on age could be discerned and this may be because of a number of processes involving both synthesis of new matrix material, as demonstrated by the increase in tissue thickness with age, and alterations in the structure of the existing matrix.

Mechanical testing showed that the lens capsule is non-linearly elastic, as noted by Krag and Andreassen (1996) and Krag et al. (1997) for porcine and human lens capsules, respectively, but conflicts with the results of Fisher (1969). The differences probably arise because the latter study employed a loading regime involving pressurisation of a membrane tethered around its perimeter, which generates a complex strain field with a maximum of 30%, compared with the uniaxial strains of up to 70% that we employed. The non-linearity of the stress–strain curve probably arises from an initial reorientation of the collagen network, followed by generation of intrafibrillar strains. Raman microspectrometry showed that even at the highest strains there were no changes in the peak position or the secondary structure of the collagen molecule as observed in type I collagen fibres (Wang et al., 2000). The polarisation changes were indicative of molecular reorientation. Further work will be required to quantify these changes but the X-ray scattering data identified a number of probable significant structural changes: the form factor ascribed to the main noncollagenous (NC1) domain was relatively isotropic in the relaxed lens capsule and with strain it became stronger in the meridional plane; the four-point pattern became obvious only with strain, and the lateral spacing of the collagen helices decreased with strain. Identification of a Raman signature of these changes should become possible in the future.

The viscoelastic response of the tissue could reflect either the time-scale of collagen network reorganisation or, and perhaps not independently, the rate of water redistribution in the tissue matrix. The studies on digested tissue indicate that glycoproteins and proteoglycans are likely to be an important determinant of either process, as has been noted in other tissues. At present, neither X-ray scattering nor Raman spectrometry has sufficient temporal resolution to enable us further to investigate the structural correlates of these transient processes.

Ageing is associated with a fall in tensile modulus and loss of viscoelasticity. Interestingly, the former is very closely compensated by the increase in tissue thickness, but the latter is not. Perhaps surprisingly it was not possible to relate the loss of organised structure with age revealed by the X-ray scattering to impaired mechanical function, in part because the anisotropy of the young tissue was not clearly reflected in its mechanical properties.

In vitro glycation produced an increase in thickness and an increase in stiffness and thermal stability in the tissue. In terms of X-ray scattering, it produced changes in matrix organisation closely resembling those of ageing but Raman microspectrometry revealed additional changes at the molecular level. Ribose and its reaction products could be detected tightly bound to the collagen fibres. There were also vibrational modes that we tentatively ascribe to the glycation cross-links which probably contribute to the mechanical changes. Whether the significant change in the secondary structure of the collagen also has mechanical consequences remains to be established.

It is uncertain whether the changes with age and glycation impair the physiological function of the lens capsule. It was employed in the present study primarily as an accessible model BM and its physiological functions have not received much attention. However, a loss of accommodation and an increase in internal pressure occur with age and in diabetes. The mechanical changes we observed are consistent with impaired intrinsic tissue properties being compensated, at least in part in older tissue, by tissue thickening. The BM of greater physiological interest is that of the vascular system. If similar mechanical changes occurred here, they would probably have extensive pathophysiological ramifications. The changes in structure, could also modify the permeability of the BM to water and solutes and thereby have further far-reaching implications.

ACKNOWLEDGEMENT

We extend appreciation to the King Salman Centre for Disability Research for providing funding via its Research Group.

REFERENCES

Ali L., Bradley D.A., Ellis R.E., Grren E., Grossmann J.G. and Winlove C.P. (2004). The structure and organisation of type-IV collagen in normal and glycated basement membrane. *Rad. Phys. Chem.,* 71, 953-956.

Banga J.D. and Sixma J.J. (1986). Diabetes melittus, vascular disease and thrombosis. *Clin. Haematol.,* 15, 465-492.

Barnard K. and Gathercole L.J. (1991). Short and long range order in basement membrane type IV collagen revealed by enzymic and chemical extraction. *Int. J. Biol. Macromol.,* 13, 359-365.

Barnard K., Gathercole L.J. and Bailey A.J. (1987). Basement membrane collagen – evidence for a novel molecular packing. *FEBS Lett*., 212, 49-52.

Basta G., Schmidt A.M. and De Caterina R. (2004). Advanced glycation end products and vascular inflammation: implications for accelerated atherosclerosis in diabetes. *Cardiovasc. Res*., 63, 582-592.

Bendall P., Koch M., Bordas J. and Rule R. (1985). *OTOKO Manual* (ICI, Runcorn).

Brodsky B. and Eikenberry K. (1985). Supramolecular collagen assemblies. *Ann. New York Acad. Sci*., 460, 73-84.

Fisher R.F. (1969). The significance of the shape of the lens and capsular energy changes in accommodation. *J. Physiol*., 201, 1-9.

Frushour B.G. and Koenig J.L. (1975). Raman scattering of collagen, gelatin and elastin. *Biopolymers*, 14, 379-91.

Gathercole L.J., Barnard K. and Atkins E.D. (1989). Molecular organization of type IV collagen: polymer liquid crystal-like aspects. *Int. J. Biol. Macromol*., 11, 335-338.

Hammersley A. (1998). *Fit2d V10.3 Reference Manual V4.0 ESRF F98HA01T*.

Heinegard D. and Sommarin Y. (1987). Isolation and characterization of proteoglycans. *Methods Enzymol.,* 144, 319-372.

Inoue S. (1994). Basic structure of basement membranes is a fine network of cords, irregular anastomosing strands. *Microsc. Res. Tech.*, 28, 29-47.

Inoue S., Leblond C.P. and Laurie G.W. (1983). Ultrastructure of Reichert's membrane, a multilayered basement membrane in the parietal wall of the rat yolk sac. *J. Cell Biol.*, 97, 1524-1537.

Kefalides N.A. (1971). Isolation of a collagen from basement membranes containing three identical α-chains. *Biochem. Biophys. Res. Commun*., 45, 226-234.

Krag S. and Andreassen T.T. (1996). Biomechanical measurements of the porcine lens capsule. *Exp. Eye. Res*., 62, 253-260.

Krag S., Olsen T. and Andreassen T.T. (1997). Biomechanical characteristics of the human anterior lens capsule in relation to age. *Invest. Ophthalmol. Vis. Sci.*, 38, 357-363.

Lefevre T., Rousseau M.E. and Pezolet M. (2007).Protein secondary structure and orientation in silk as revealed by Raman spectromicroscopy. *Biophys. J*., 92, 2885-2895.

Menzel E.J. and Reihsner R. (1991). Alterations of biochemical and biomechanical properties of rat tail tendons caused by non-enzymatic glycation and their inhibition by dibasic amino acids arginine and lysine. *Diabetologia,* 34, 12-16.

Paulsson M., Aumailley M., Deutzmann R., Timpl R., Beck K. and Engel J. (1987). Laminin-nidogen complex: extraction with chelating agents and structural characterization. *Eur. J. Biochem*., 166, 11-19.

Rippe K., Mücke N. and Langowski J. (1997). Superhelix dimensions of a 1868 base pair plasmid determined by scanning force microscopy in air and in aqueous solution. *Nucleic Acids Res*., 25, 1736-1744.

Sane S.U., Cramer S.M. and Przybcien T.M. (1999). A holistic approach to protein secondary structure characterization using amide I band Raman spectroscopy. *Anal. Biochem.*, 269, 255-272.

Siebold B., Deutzmann R. and Kuhn K. (1987). The arrangement of intra and intermolecular disulfide bonds in the carboxyterminal, noncollagenous aggregation and cross-linking domain of basement membrane type IV collagen. *Eur. J. Biochem.,* 176, 617-624.

Timpl R. (1989). Structure and biological activity of basement membrane proteins. *Eur. J. Biochem*., 180, 487-502.

Timpl R. and Dziadek M. (1986). Structure, development and molecular pathology of basement membranes. *Int. Rev. Exp. Pathol*., 29, 1-112.

Tsilibary E.C. and Charonis A.S. (1986). The role of the main noncollagenous domain (NC I) in type IV collagen self-assembly. *J. Biol. Chem*., 103, 2467-2473.

Vries A. (1970). X-ray photographic studies of liquid crystals. *Mol. Cryst. Liq. Cryst*., 10, 219-236.

Wang Y-N., Galiotis C. and Bader D.L. (2000). Determination of molecular changes in soft tissues under strain using laser Raman microscopy. *J. Biomech*., 33, 483-486.

Winlove C.P., Parker K.H., Avery N.C. and Bailey A.J. (1996). Interactions of elastin and aorta with sugars *in vitro* and their effects on biochemical and physical properties. *Diabetologia,* 39, 1131-1139.

Yurchenco P.D. and Furthmayr H. (1984). Self-assembly of basement membrane collagen. *Biochem*., 23, 1839-1850.

Yurchenko P.D. and O'Rear J. (1993). In: *Molecular and Aspects of Basement Membrane* (Rohrbach D. and Timpl R., eds.) pp. 19-47, Acad. Press, New York.

Yurchenco P.D. and Ruben G.C. (1987). Basement membrane in situ: evidence for lateral association in the type IV collagen network. *J. Cell Biol*., 105, 2559-2568.